WAVE-SOLID INTERACTIONS IN SHOCK INDUCED DEFORMATION PROCESSES

Paper #1003

Yajun Fan, Youneng Wang, Sinisa Vukelic, Y. Lawrence Yao

Department of Mechanical Engineering, Columbia University
New York, NY 10027, USA

Abstract

A model was developed for material deformation processes induced by laser generated shock waves. The processes include laser peen forming (LPF) and laser shock peening (LSP) of metals. Numerical solutions of the model using finite element method (FEM) were implemented in two steps: (1) explicit step, devoted to shock wave propagation; and (2) implicit step, calculating relaxation of material. A series of LPF and LSP experiments were conducted to validate the model. The residual stress measurements by synchrotron X-ray diffraction and deformation measurements by profilometry showed that the experimental and numerical results were in good agreement. An important aspect of the work is that the numerical results were further analytically explored to gain improved understanding of wave-solid interaction including shock wave attenuation and shock velocity variation.

Introduction

Shock waves are characterized in that the wave front, in which compression takes place, is a region of sudden and violent change in material velocity, stress, and density. Since the first experiments in the 1960s utilizing high power pulsed lasers to generate shock waves in solid targets, the laser shock technique has led to many investigations, including laser peen-forming (LPF) and laser shock peening (LSP), shown as in Fig. 1.

Laser-generated shock waves result from the expansion of a high pressure plasma caused by a pulsed laser. An intense laser pulse interacting with a solid target immediately causes the surface layer instantaneously vaporizes into a high temperature and high pressure plasma. This ablated plasma expands from the surface and, in turn, exerts mechanical pressure on the face of the target, which induces compressive waves in the solid target, and therefore a shock wave is propagated through the sample. If it is confined by liquid or another type of laser transparent medium, the shock pressure can be magnified by a factor 5 or more compared with the open-air condition. The coating also protects the target from thermal effects so that nearly pure mechanical effects are induced. LSP is an innovative process in which beneficial compressive residual stress is imparted into the processed surface layer of metal or alloy parts by laser generated shocks, and the process has been extensively investigated and in some cases successfully applied[1-2]. When the peak pressure created by the shock wave is above the dynamic yield stress (Hugonoit Elastic Limit, HEL) of metal, the metal is plastically deformed at the surface which will induce compressive residual stress in the surface of the part and thus increase the resistance of the metal to surface related failures such as fatigue, fretting fatigue, and stress corrosion cracking. LSP is only a surface treatment method, and does not produce appreciable change of shape. LPF is a new process involving laser generated shock waves. It combines the beneficial effects (compressive residual stresses on the surface) of a LSP with a controlled bending deformation, to shape parts [3]. The process is more effective than other forming methods with a distinct advantage that surface stresses generated can be compressive. Therefore, the process results in increased fatigue resistance of the target material in addition to shaping it. However, to advance LSP and LPF in particular, the answers to some questions, for example, how to control the repetition rate in a multiple-pulsed laser processing, how to determine the pulse duration considering the thickness of parts during LPF, and in two sided LSP, how to design the phase difference between the two shock waves in order to gain an optimal effect, need to be further investigated. These questions are closely related to the shock-solids interactions, such as shock wave attenuation, reflection and variation of shock wave velocity.

Numerical modeling is an effective way to understand shock-solids interaction. Shock wave propagation in solids has been numerically investigated. Mok[4] simulated the propagation and attenuation of spherical and plane shock waves in a 2024 aluminum plate by

assuming that the media is a strain-rate-independent and elastic-perfectly plastic solid. Caruso, et al.[5] also numerically investigated laser-generated shock propagation dynamics in the solids, but only an elastic medium in plane geometry was considered. Shock-solid interaction was also simulated in some studies of spallation and residual stresses induced by LSP[6-7], but the effect of high strain rate was not considered or fully considered only by the Johnson-Cook law. Most studies on the shock-solid interaction provide few practical directions for the application of material deformation processes induced by laser generated shock waves.

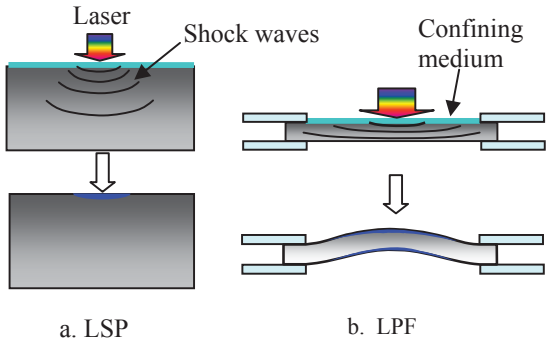

Fig. 1 Material deformation processes induced by laser generated shock waves: (a) Laser Shock Peening (LSP) causes compressive residual stress on the processed surface; (b) Laser Peen Formig (LPF) forms the sheet, imparting compressive residual stress on both surfaces

In this work, an explicit/implicit FEM model is developed to simulate material deformation processes induced by laser-generated shock waves. Explicit dynamic analysis is implemented for shock wave propagation in strain-rate dependent and elastic-plastic solids, and implicit analysis is applied for relaxation of pressured materials. The resultant plastic deformation and residual stress fields can be then calculated. The model is validated by comparing the calculated deformation and residual stress fields with deformation measurements by profilometry and the residual stress measurements by synchrotron X-ray diffraction. The numerical results were further analytically explored to gain improved understanding of wave-solid interaction including shock wave attenuation and shock velocity variation.

Physical Process & Governing Equations

When a high pressure is suddenly applied to a metallic target, the pressure is accumulated in the wave front because it can not disperse away within such a short time, and the wave front becomes steeper and steeper, and finally evolves into an almost discontinuous jump. Shock wave is then formed. Because the pressure is accumulated, the shock front is highly compressive, which also causes the discontinuity of density, stress and other quantities between shock wave front and the unshocked region. The shocked solids are thought to have a fluidlike hydrodynamic deformation under such a high pressure, but solids are still different from liquids in that solids have material strength and plastic flow, and their deformation behavior is related to strain and strain rate in particular.

Laser-generated Shock Loading

A model was previously developed for the prediction of laser-generated pressure in the confined ablation mode [8]. It considered the mass, energy and momentum exchanges between plasma and confining medium or plasma and metallic target. The expansion of plasma was modeled as one dimensional laser-supported combustion wave. Figure 2 presents the calculated laser-generated shock loading profiles under different processing conditions. The calculated shock loading was used in the later shock wave propagation simulation as input and was assumed to be of a spatially Gaussian distribution.

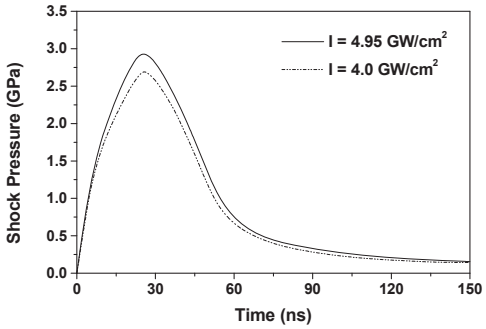

Fig. 2 The loading history based on a former model [9].

Hydrostatic and Deviatoric Behaviors

The precise numerical description of a LPF or LSP process requires the simulation take into account the hydrodynamic behavior of the material and the deviatoric behavior considering work hardening and strain rate effects. The calculations of dynamic behavior of condensed matter under shock loading was made using the three conservation equations of mass, momentum, and energy. But these conservation laws can not completely govern the behavior of solids under shock loading. When the applied stress greatly exceeds the yield stress of a solid, its behavior is more complicated, and can be approximated by a fluidlike one because the fractional deviations from stress isotropy are small. The complete process of shock wave propagation in solids should be governed by the

three conservation equations, equation of state that can be expressed in terms of specific internal energy as a function of pressure and density for hydrodynamic behavior of material, and the elastic-plastic constitutive relation for deviatoric behavior.

The calculation of mechanical behavior of solids under shock loading is usually made using the three conservation equations in integral forms:

$$\frac{d}{dt}\oint_V \rho dV = 0 \qquad (1)$$

$$\frac{d}{dt}\oint_V \rho u_i dV = \oint_S \sigma_{ij} u_j dS \qquad (2)$$

$$\frac{d}{dt}\oint_V \rho(E + \frac{1}{2}u^2)dV = \oint_S \sigma_{ij} n_{jk} u_k dS \qquad (3)$$

where V is the volume of a cell, S is the surface that covers this volume, n_{ij} is the unit vector normal to this surface, u_i are the velocity components, and σ_{ij} are the stress components. The elasto-plastic behavior should also be considered except the hydrodynamic change of volume or density. The stress-tensor components are divided into a hydrostatic equation of state and an elastic-plastic constitutive model. The stress components σ_{ij} can be written as:

$$\sigma_{ij} = -P + s_{ij} \qquad (4)$$

where P is the hydrostatic pressure and s_{ij} is the deviatoric stress components.

A commonly used equation of state for solids is the Mie-Grüneisen equation of state. The Mie-Grüneisen equation of state which establishes relationship between pressure P and internal energy E with reference to the material Hugoniot curve, was used:

$$P - P_H = \gamma_0 \rho_0 (E - E_H) \qquad (5)$$

where P_H and E_H are the Hugonoit pressure and internal energy, γ_0 is a material constant and ρ_0 represents the initial state density.

The Hugonoit curve is described by the linear relation between the shock velocity U and particle velocity u with coefficients from experimental data:

$$U = C_0 + Su \qquad (6)$$

where the constant C_0 is the sound speed at zero pressure, and the material constant s has a value between 1.0 and 1.7 for most metals.

Combining equation (6) with the Rankine-Hugonoit jump conditions [9], the Hugonoit pressure and internal energy can be obtained as:

$$P_H = \frac{\rho_0 C_0 \eta}{(1 - S\eta)^2} \qquad (7)$$

$$E_H = \frac{P_H \eta}{2\rho_0} \qquad (8)$$

and substituting equation (7) and (8) into equation (5) yields:

$$P = \frac{\rho_0 C_0 \eta}{(1 - S\eta)^2}(1 - \frac{\gamma_0 \eta}{2}) + \gamma_0 \rho_0 E \qquad (9)$$

where $\eta = 1 - \frac{\rho_0}{\rho}$, and ρ is density. The equation (9) is the final form of equation of state to be used in this simulation. In the following numerical modeling of shock-solid interactions, work hardening, strain rate and pressure effects on yield strength are considered while temperature is taken as room temperature. This is reasonable because only the coating is vaporized and minimal thermal effects are felt by the sample. The solid target is assumed to be isotropic.

Numerical Modeling

FEM Explicit & Implicit Modeling

The commercial finite element solver, ABAQUS/Explicit and ABAQUS/Standard, were combined to perform the LSP and LPF simulation. These two solvers accomplish different calculations during this simulation. The ABAQUS/Explicit is a non-linear explicit time integration finite element code, which is especially well suited for solving high speed, short duration, highly dynamic events that require many small time step increments to obtain a high resolution solution. One important issue about the simulation of LPF and LSP is the balance between a short time for dynamic shock-solid interaction (2~3 times of the laser pulse duration) and a much longer relaxation time (up to 1 second) to reach a stabilized mechanical state. So the ABAQUS/Explicit code is first applied to simulate the dynamic shock-solid interaction process. But the ABAQUS/Explicit method is only conditionally stable and very small time step is required. Therefore, the second step is to simulate material relaxation in ABAQUS/Standard. As soon as the calculation of the highly dynamic shock-solid interaction process is completed in ABAQUS/Explicit, the obtained intermediate stress and strain state is transferred into ABAQUS/Standard to simulate the material relaxation and get the residual stress filed in static equilibrium. In the ABAQUS/Explicit step, a small amount of damping in a form of bulk viscosity (=0.06) is included in the calculation to limit numerical oscillations.

Strain Rate Dependent Considerations

In LPF and LSP, the target is subjected to very strong shock pressures (>1 GPa), the interaction time is very short (<200 ns), and the strain rate is very high (>100,000 s^{-1}). It is necessary to consider the effect of high strain rate on the flow behavior of metals. Johnson, et al.[10] first included the influence of strain rate $\dot{\varepsilon}$ into their working hardening model. But Johnson's model[22] could not cover the high strain rate (greater than 10^{-6} s^{-1}) in LPF and LSP. It did not also consider pressure effects, which are very important in laser shock processing. Steinberg's model [11] is applicable to ultrahigh pressures but it did not consider rate dependent effects. It was found that the rate dependent effects cannot be neglected for shock pressures below 10 GPa. In laser shock processing, the pressure involved is fairly high (>1 GPa) but less than 10 GPa.

For laser shock processing, therefore, both the strain rate effects and ultrahigh pressure effects on material yield stress need to be considered. A prior research[5] has included the strain rate (even above 10^6 s^{-1}) effects and ultrahigh pressure effects on material yield stress, and the obtained dynamic yield stress data were used in this research.

Experiments

Laser and Sample Preparations

All experiments were made by a frequency tripled Q-switched Nd:YAG laser with a wavelength of 355nm in TEM00 mode. The pulse duration was 50 ns, and pulse repetition rate could vary between 1 KHz to 20 KHz. Laser beam diameter is 12 microns and laser intensity was varied from 2 to 6 GW/cm2.

For LPF, copper stripes with thickness of 100μm were used as samples. These stripes were cut to 20mm×3mm using a wire electric discharge machine (EDM) to avoid inducing stress and strain, and then heat treated and electro-polished to relieve residual stress. Then, a thin layer of high vacuum grease (about 10 microns) was spread evenly on the polished sample surface, and the coating material, aluminum foil of 16 microns thick, which was chosen for its relatively low threshold of vaporization, was tightly pressed onto the grease. These stripes were clamped at both ends, leaving 10 mm length in the middle unsupported for LPF experiments. Caution was exercised to pre-bending effects and to ensure these stripes remain flat during these steps .

For LSP, well-annealed pure aluminum samples in the dimension of 15mm×10mm×5mm were used. The sample preparation was the same as introduced before[3].

For both LPF and LSP, the laser process procedure is similar. The samples were placed in a shallow container filled with distilled water around 3 mm above the sample top surface. A series of laser pulses were applied along the width direction (the dimension of 3 mm for LPF and the dimension of 10 mm for LSP) with 25 μm spacing between adjacent pulses. This forms a straight shocked line. Pulse energies, 226 and 280μJ, corresponding to laser intensities of 4.0 and 4.95GW/cm^2, were used for LPF and LSP, respectively. After shock processing, the coating layer and the vacuum grease were solved in Acetone solution, and shock induced deformation and residual stresses on the samples were measured. The conditions are summarized in Table 1.

Table. 1 Samples and Experimental Conditions for LPF and LSP.

	Material	Size (mm^3)	Laser Intensity (GW/cm^2)	Pulse Energy
LPF	Cu	10×3×0.1	4.95	280 μJ
LSP	Al	15×10×5	4.0	226 μJ

Deformation & Residual Stresses Measurements

Before and after LPF, the curvatures of the stripes were measured by a profilometer, and the bending caused by LPF is the net effect, as shown in Fig. 3. After LSP, the dented surface was measured using Atomic Force Microscopy (AFM).

The residual stresses were measured by synchrotron X-ray diffraction. Synchrotron X-ray diffraction can make accurate residual stress measurement of a high spatial resolution because it provides high brightness X-ray beams. The extremely high brightness X-ray beams from synchrotron radiation sources are narrowed down and then focused to micron or submicron spot sizes using X-ray optics such as Fresnel Zone Plates (FZP) or tapered glass capillaries, and either white beam or monochromatic X-rays can be used. The tapered capillary tube is aligned to take in the X-ray beam from the synchrotron beamline, and successively focuses the beam to a small spot size by total external reflection. Both small spot size and increased intensity are desired in X-ray diffraction with a micron-level spatial resolution.

The samples are mounted on a translation stage with positioning accuracy of ±1μm in the x and y directions in the sample surface. Monochromatic synchrotron radiation at 8.0 KeV ($\lambda = 1.54024\,\text{Å}$) is used, since it is smaller than the K absorption edge for Al and Cu

which are 8.98KeV and 8.3KeV so that the fluorescence radiation would not be excited.

Multiple measurement points were chosen along a line perpendicular to the shocked line. The spacing between adjacent measurement points starts from 20 μm (when ±100 μm away from the center of the shocked line) and reduces to 5 μm within ±20 μm from the center of the shocked line in order to spatially resolve the residual stress. At each position, the corresponding X-ray diffraction profile is recorded and repeated for each shocked line. For LSP, only the shocked surface was measured while for LPF, the residual stresses measurements on both top and bottom surfaces were conducted.

Results and Discussions

Model Validation

Comparison with experimental results

The comparison between the measured deformation of the copper stripe after LPF and the numerical predicted is shown in Fig. 3. Before laser peen forming, the stripe slightly curves upward with the center of the stripe up by about 5 microns. After LPF, the stripe bended upward further, and the shocked area was raised by up to 10 microns. The numerically predicted deformation and the experimental are in good agreement.

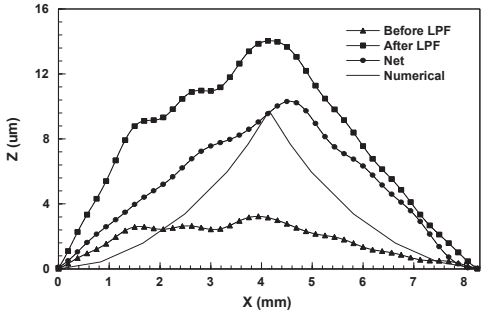

Fig. 3 Comparisons of deformation after LPF between the experimental and the numerical results.

Fig. 4 recorded X-ray diffraction profiles along a line perpendicular to the shocked line. In Fig. 4, when the measured location is far from the shocked line (> 100μm or < -100μm), X-ray diffraction profile is single symmetric peak, and the measured Bragg angle is around 25.16°, the theoretical Bragg angle for Cu (002) reflection, which indicates the measured location is within the shock free regions. When the measured location gets closer to the shocked line, the peak shifts towards smaller diffraction angles, meanwhile, the X-ray diffraction profile is broadened or a second peak pops up towards larger diffraction angle. The full width at half maximum (FWHM) of the profile around the shocked line is up to 3 times greater than that of the line profile at 100μm away from the center. It is known that when both elastic and plastic strains are superposed in plastically deformed metals, diffraction is both shifted and broadened. It is the superposition that makes it difficult to evaluate the local strain and residual stress distribution. However, on the basis of a composite model [12], local strain and residual stress can be evaluated for metals under plastic deformation by recognizing that the crystal dislocations often arrange themselves in a cell structure after being subjected to a shock loading. Following the analysis method above for each measurement point, the spatially resolved residual stress distributions on both top and bottom are shown in Fig. 5. The comparisons of the residual stress distributions on both top and bottom show the numerically predicted distribution matches the experimental results very well. The modeled residual stress distribution and bending induced by LPF of copper stripe are also shown in Fig. 6. When high pressure was applied to the copper, the shocked material tended to flow away from the shocked center and caused elongation of the top layer of the stripe, which led the stripe to bend up, and meanwhile induced compressive residual stress on the bottom surface and, because of spring back and shock compression, the top surface.

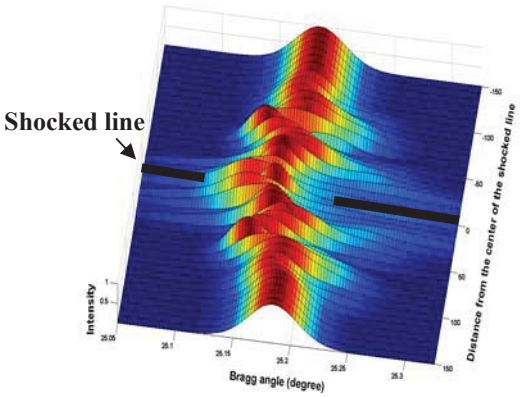

Fig. 4 3D X-ray profile spatial distribution across the shocked line for (002) reflection of copper sample: distance from the shocked line center in μm.

Fig. 7 shows that the comparison between the AFM measured dent on the shocked area after LSP of bulk aluminum sample and the FEM calculated. The X-ray microdiffraction measured residual stresses distribution induced by LSP and the numerically obtained residual stress field are showed in Fig. 8. Both Fig. 7 and Fig. 8 show a good agreement between the experimental and the numerical.

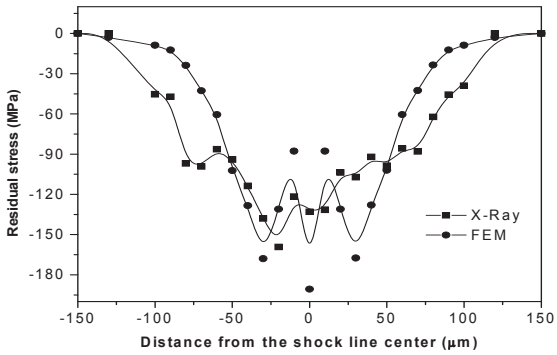

(a)

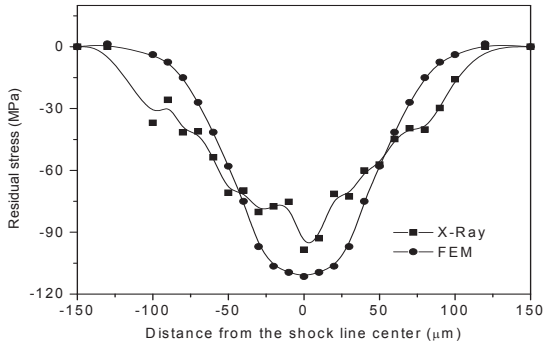

(b)

Fig. 5 Comparison between the experimental and the numerical residual stresses induced by LPF of copper stripes with thickness of 100 μm: (a) Top surface; and (b) Bottom.

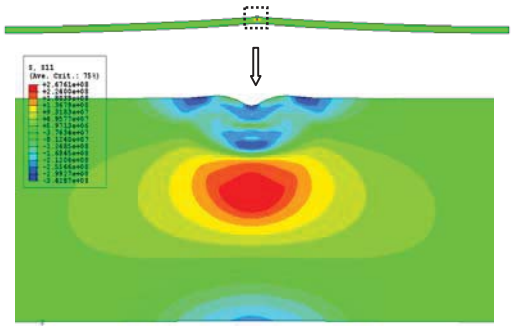

Fig. 6 The simulated deformation and residual stresses field induced by LPF. The deformation of the stripe is magnified 10 times for viewing clarity. S11 is residual stress along the sample top surface.

Steady shocks structure

The peak pressure of a laser-generated shock loading applied for LPF and LSP is generally in the range from 1GPa to 10GPa, which is in the elastic-plastic shock regime. The elastic-plastic shock regime is characterized by a two-wave structure with an elastic precursor followed by a plastic wave, which further compresses the material to the final state. The transition from an elastic precursor to the following plastic wave occurs within a thin layer, which is also called the plastic shock front, where the material rapidly deformed. The two-step shock wave profile has been verified by a series of experiments [13]. To numerically obtain a steady planar shock wave, a uniform pressure loading with a duration time of 50 ns is applied. Fig. 9 shows that the calculated shock wave profiles at 50 ns and 100 ns. When t = 50 ns, unloading just starts, so there is no rarefaction wave; when t = 100 ns, a steady shock wave with a rarefaction wave moving in the same direction is obtained, and both shock front and rarefaction wave are characterized by elastic and plastic response with a two step profile. The numerically obtained steady shock wave structure matches the theoretical and experimental analysis made by Lipkin and Asay[13].

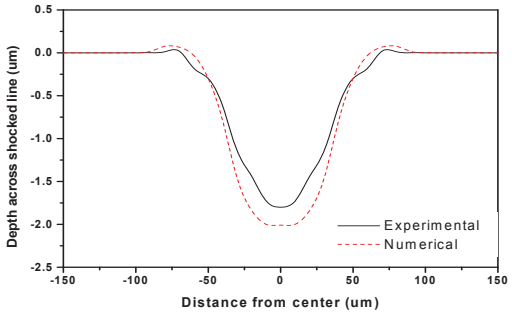

Fig. 7 Comparison of measured and simulated dents across the shocked line after LSP of Al sample.

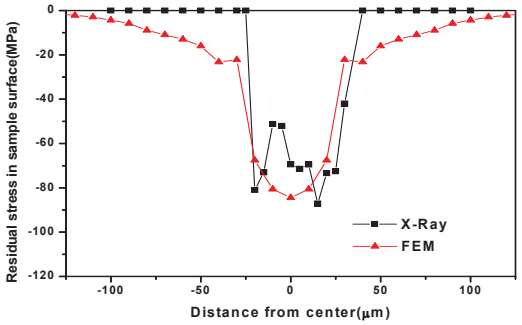

Fig. 8 Comparison between the measured residual stresses distribution induced by LSP on the shocked surface of Al sample with the numerical result.

The above comparison and wave profile analysis demonstrate that the proposed numerical method is a satisfactory one for solving shock-solid interaction problems. Based on the model, shock wave velocity variation, attenuation, and effect of strain rate are then further explored.

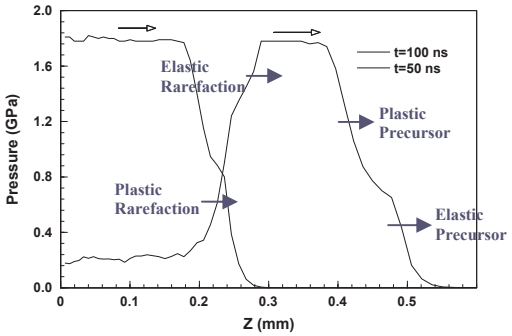

Fig. 9 The numerically obtained structure of steady shock wave: laser pulse duration time = 50ns.

Shock Wave Velocity Variations

It is well known that shock wave velocity in solid is relative to stress or pressure. During shock wave propagating in a metal plate, shock velocity varied as the changing stress states. A one dimensional shock wave motion is considered. The governing equations in Lagrangian form are

$$\rho_0 \frac{\partial u}{\partial t} = \frac{\partial \sigma}{\partial X} \quad \text{(Momentum conservation)}$$
$$\frac{\partial u}{\partial X} = \frac{\partial \varepsilon}{\partial t} \quad \text{(Mass conservation)} \qquad (10)$$

where X is the Lagrangian displacement, σ and ε are the stress and strain, respectively.

Assuming a stress-strain constitutive relation $\sigma = \sigma(\varepsilon)$, neglecting the effect of strain rate, and that particle velocity u is a single valued function of σ, the equation (10) can be rewritten as:

$$\rho_0 \frac{\partial u}{\partial \sigma}\frac{\partial \sigma}{\partial t} = \frac{\partial \sigma}{\partial X}$$
$$\frac{\partial u}{\partial \sigma}\frac{\partial \sigma}{\partial X} = \frac{\partial \varepsilon}{\partial \sigma}\frac{\partial \sigma}{\partial t} \qquad (11)$$

Solving equations (11) yields

$$\rho_0 \left(\frac{\partial u}{\partial \sigma}\right)^2 = \frac{\partial \varepsilon}{\partial \sigma} \qquad (12)$$

Based on equation (12), a characteristic speed of propagation can be expressed as:

$$U(\sigma) = \frac{1}{\rho_0 \frac{\partial u}{\partial \sigma}} = \sqrt{\frac{1}{\rho_0}\frac{\partial \sigma}{\partial \varepsilon}} \qquad (13)$$

If the shock wave is a linear elastic wave, the wave speed is constant based on equation (13). For a typical shock wave in LSP or LPF, the stress-strain constitutive relation is more complicated considering plastic deformation and work hardening. According to Johnson-Cook law, an elastic- plastic constitutive relation, including effects of work hardening and strain rate, can be expressed as:

$$\sigma = (A + B\varepsilon^n)\left(1 + C\ln\left(\frac{\dot{\varepsilon}}{\dot{\varepsilon}_0}\right)\right) \qquad (14)$$

where A, B, C and n are material constants (for example, A = 120 MPa, B = 300 MPa, n = 0.35 and C = 0.1 for pure aluminum), ε is equivalent plastic strain, $\dot{\varepsilon}$ and $\dot{\varepsilon}_0$ are strain rate and the strain rate under quasi-static loading. If the strain rate effect is neglected, equation (14) can be rewritten as:

$$\sigma \approx (A + B\varepsilon^n) \qquad (15)$$

Substituting equation (15) into equation (13) leads to

$$U(\varepsilon) = \frac{1}{\rho_0 \frac{\partial u}{\partial \sigma}} = \sqrt{\frac{1}{\rho_0}\frac{\partial \sigma}{\partial \varepsilon}} = \sqrt{\frac{Bn}{\rho_0}\varepsilon^{n-1}} \qquad (16)$$

Because n is smaller than unity and B is positive for most metals, the equation (16) shows that the wave velocity varies with strain: the larger the strain is, the smaller the shock wave velocity.

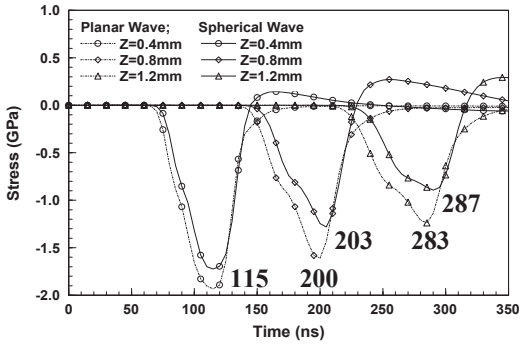

Fig. 10 The calculated time history of stress at three locations below the shocked surface (X=0 mm) along the thickness direction for both planar shock wave and spherical shock wave.

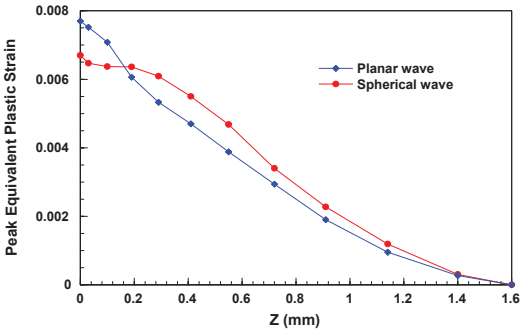

Fig 11 The calculated peak equivalent plastic strain along the thickness of the copper plate.

To investigate the variation of shock wave velocity during propagation, the simulation of a planar shock

wave propagating in a copper plate with thickness of 1.6 mm is run based on this proposed model. A uniform pressure loading with duration time of 50 ns are applied to produce a planar shock wave, while a Gaussian distributed pressure loading with a small effective radius of 0.5 mm are exerted on the top surface of the copper plate to get a spherical shock wave. Fig. 10 shows the calculated stress history at Z = 0.4 mm (1/4 thickness), Z = 0.8 mm, and Z = 1.2 mm of the copper plate for both planar shock and spherical shock cases. From Fig.10, the average shock velocity within each ¼ of thickness can be calculated in terms of the time corresponding to the peak stress at those locations. For the planar shock, the average plastic wave velocity within the first 0.4mm is about 4.4 km/s (= 0.4mm/(115-25) ns, 25 ns is half of the pressure duration time), 4.7 km/s (=0.4mm/(200-115) ns) within the second 0.4mm, and 4.8 km/s (=0.4mm/(283-200) ns) within the third 0.4mm. For spherical shock wave, it is also shown that the plastic wave speed increases as it is propagating. Comparing the plastic wave speed of the planar wave with that of the spherical wave, it is found that they are the same within the first 0.4 mm, and later on the spherical wave propagates faster than the planar wave. This can be explained by Equation (16). The equation (16) shows that the larger the strain is, the smaller the shock wave velocity. The calculated peak plastic strain along the thickness of the copper plate is shown in Fig. 11, which demonstrates a decreasing equivalent peak plastic strain, therefore based on equation (16), the plastic wave speed increases. Moreover, Fig. 11 shows that the equivalent peak plastic strain within the initial 0.2 mm in the planar wave propagation is larger than that in the spherical shock propagation, and after that it becomes less due to greater strain rate hardening, which also explains why the spherical wave propagates faster than the planar wave after the first 0.4 mm.

Attenuation of Planar and Spherical Shock Wave

For a LSP process as a surface treatment method, the thickness of part is generally large compared with the treated area and the part is thus often thought to be a semi-infinite body and the driven shock wave thought to be spherical. While for a LPF process, the sheet has a smaller thickness relative to laser spot size to be formable, therefore the driven shock wave in LPF can be reasonably assumed to be planar wave. As informed before, the shock wave attenuations directly determine the selection of some processing parameters, like pulse duration time and duty cycle in laser processing involving multiple pulses.

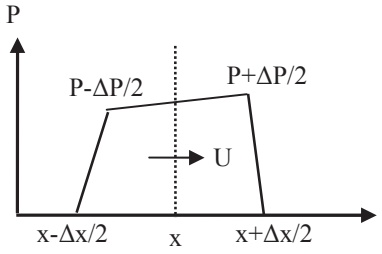

Fig. 12 Schematic of a single centered shock wave

Assuming a centered single shock wave is propagating, shown as in Fig. 12. The center of the shock wave is at x with pressure P, and the leading and tailing edges of the shock are at $(x+\Delta x/2)$ and $(x-\Delta x/2)$ with pressure $(P+\Delta P/2)$ and $(P-\Delta P/2)$, respectively. The width of the shock wave at x is Δx. Based on the above assumptions, when the shock wave propagates for a short distance from x_0 to x, the attenuation of particle velocity of planar shock wave and spherical shock wave can be expressed as (the derivation is given in Appendix):

$$\frac{u(x)}{u(x_0)} = \exp(-K_P(x-x_0)) \quad \text{(planar wave)} \quad (17)$$

$$\frac{u(x)}{u(x_0)} = \frac{x_0}{x}\exp(-K_S(x-x_0)) \quad \text{(spherical wave)} \quad (18)$$

where $\Delta P = P(x+\Delta x/2) - P(x-\Delta x/2)$ and $K_S = K_P = \frac{1}{2\Delta x}(\frac{\partial U}{\partial P})\frac{\Delta P}{U}$. When the shock wave moves from x_0 to x, we have $(\frac{x_0}{x} > 1)$. Comparing the equation (17) and (18), it is found that the spherical wave decays faster than planar wave under the same conditions due to greater geometrical dissipation of energy. Therefore, comparing LPF of a thin plate in which a planar shock wave is assumed to generate, with LSP of a thick plate in which the laser driven shock is thought to be spherical wave, the pulse repetition rate in LPF should be lower than that in LSP. In addition, attenuation of planar wave and spherical wave is also relative to the value of K_S or K_P. $\frac{\partial U}{\partial P} > 0$ is a necessary condition to form a shock wave and its value is only dependent on the elastic property and inertial property of media, and meanwhile *U* and Δx are assumed to be constant, therefore, the value of K_S or K_P is only dependent on ΔP. Clearly, the ΔP during loading is less than that during unloading, therefore, the attenuation during loading is slower than that during unloading. Fig. 13 shows the simulated attenuation of shock wave propagating in the copper plate with thickness of 1.6 mm, and loading duration

time is 50 ns. It is found that the shock waves decay very slowly near the shocked top surface. The numerical results also demonstrate that for both planar shock wave and spherical shock wave the attenuation during loading is much slower than that during unloading. From the numerical results, the attenuation of shock wave during loading appears to be linear, and the slope for planar wave is smaller than that for spherical wave; during unloading the attenuation appears to be exponentially decaying.

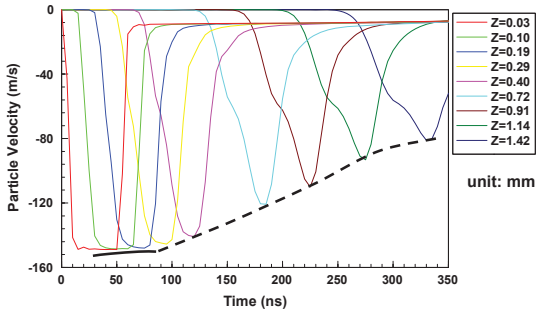

(a) Planar wave

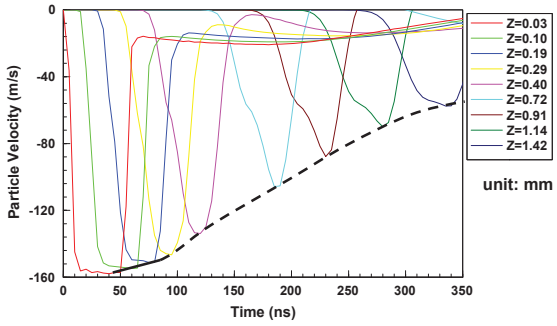

(b) Spherical wave

Fig. 13 The simulated attenuation of particle velocity of shock waves: (a) planar shock wave; and (b) spherical shock wave. Laser pulse duration time is 50 ns. When t = 50 ns, the shock wave already reached at Z = 0.19 mm, so the loading region is from Z = 0 mm to Z ≈ 0.2 mm.

The above discussion only considers the attenuation of shock wave due to geometry and loading conditions. It is known that attenuation of shock wave is also affected by plastic deformation, and interaction between rarefaction wave and shock wave.

Note that the velocity near the shocked top surface is about twice the speed at interior locations because the free surface generates a reflected wave travelling in the opposite direction. As in the case of the stress-time profiles, the HEL becomes more discernible with increase in propagation distance from the shocked top surface. This is due to the fact that the plastic wave propagates slower than the elastic precursor and thus the two waves tend to separate with increase in propagation distance.

Conclusions

A FEM model to simulate shock wave propagation in solids is proposed to calculate induced deformation and residual stress fields in laser peen forming (LPF) and laser shock peening (LSP). The experimental measurement of deformation and residual stress fields showed an good agreement with the numerical results. Based on this model, the variation of shock wave velocity and attenuation in LPF and LSP are further analyzed, respectively. Both analytical and numerical results show that shock wave velocity is affected by equivalent plastic strain when the shock wave is in the plastic regime, and that attenuation of shock waves in LPF and LSP is dependent on loading states. Those results can be very useful in exploring and designing applications of LPF and LSP.

Acknowledgments

The authors gratefully acknowledge the assistance in X-Ray microdiffraction experiments from Dr. J. L. Jordan-Sweet, Brookhaven National Laboratory.

Appendix

A centered single shock wave is propagating, shown as in Fig. 5. The center of the shock wave is at x with pressure P, and the leading and tailing edges of the shock are at $(x+\Delta x/2)$ and $(x-\Delta x/2)$ with pressure $(P+\Delta P/2)$ and $(P-\Delta P/2)$, respectively. The width of the shock wave at x is Δx. When the shock wave moves to $(x+dx)$, the location x_+ of the leading edge can be expressed as:

$$x_+ = x+\Delta x/2+\left(\frac{\partial U}{\partial P}\frac{\Delta P}{2}\right)\frac{dx}{U} \qquad \text{(A1)}$$

Meanwhile, the location x_- of tailing edge is

$$x_- = x-\Delta x/2+\left(-\frac{\partial U}{\partial P}\frac{\Delta P}{2}\right)\frac{dx}{U} \qquad \text{(A2)}$$

where $\Delta P = P(x+\Delta x/2)-P(x-\Delta x/2)$. Terefore, the location of center of the shock wave at $(x+dx)$ can be expressed as following:

$$\Delta x(x+dx) = x_+ - x_- = \Delta x(x)+\frac{\partial U}{\partial P}\frac{\Delta P dx}{U} \qquad \text{(A3)}$$

or

$$\frac{d\Delta x}{dx} \approx \frac{\Delta x(x+dx)-\Delta x(x)}{dx} = \frac{\partial U}{\partial P}\frac{\Delta P}{U} \qquad \text{(A4)}$$

If only considering kinematic energy of the shock wave, energy conservation for a planar shock wave gives

$$\Delta x u^2 = \text{Const} \qquad \text{(A5)}$$

While for a spherical shock wave, energy conservation yields

$$x^2 \Delta x u^2 = \text{Const} \qquad \text{(A6)}$$

Differentiating equation (A5) and (A6), respectively, leads to:

$$\frac{du}{dx} = -\frac{ud\Delta x}{2\Delta x dx} \quad \text{(planar wave)} \qquad \text{(A7)}$$

$$\frac{du}{dx} = -\frac{u}{x}\left(1+\frac{xd\Delta x}{2\Delta x dx}\right) \text{ (spherical wave)} \qquad \text{(A8)}$$

Substituting equation (A4) into equation (A7) and (A8), respectively, yields

$$\frac{du}{dx} = -uK_P \quad \text{(planar wave)} \qquad \text{(A9)}$$

$$\frac{du}{dx} = -\frac{u}{x}(1+xK_S) \quad \text{(Spherical wave)} \qquad \text{(A10)}$$

where $K_S = K_P = \frac{1}{2\Delta x}\left(\frac{\partial U}{\partial P}\right)\frac{\Delta P}{U}$. K_S and K_P are relative to *U*, *P*, and Δx. If the shock wave propagate a short distance from x_0 to x, K_S and K_P can be approximately assumed to be constant. Thus, integrating equation (A9) and (A10) yields the equation (17) and (18).

References

[1] Clauer, A. H. and Holbrook, J. H. (1981) Effects of laser induced shock waves on metals, Shock Waves and High Strain Phenomena in Metals-Concepts and Applications, New York, Plenum, 675-702.

[2] Peyre, P. *et al.* (2003) FEM simulation of residual stresses induced by laser peening, Eur. Phys. J. AP 23, 83-88.

[3] Zhou, M., Zhang, Y. and Cai, L. (2002) Laser shock forming on coated metal sheets characterized by ultrahigh strain rate plastic deformation, J. App. Phys. 91(8), 5501-5503.

[4] Chi-Hung, Mok (1968) Effects of solid strength on the propagation and attenuation of spherical and plane shock waves, J. App. Phys. 39, 2072-2081.

[5] Caruso, A., Guskov, S. Y., Doskach, I. Y., Zmitrenko, N. V., Rozanov, V. B. and Strangio, C. (2001) Laer-generated weak shock wave propagation dynamics in the solids, Proc. SPIE 4424, 508-511.

[6] Cottet, F. and Boustie, M. (1989) Spallation studies in aluminum targets using shock waves induced by laser irradiation at various pulse durations, J. App. Phys. 66(9), 4067-4073.

[7] Ocana, J. L., Morales, M., Molpeceres, C., Torres, J. (2004) Numerical simulation of surface deformation and residual stresses fields in laser shock processing experiments, Applied Surface Science 238, 242-248.

[8] Zhang, W. and Yao, Y. L. (2000) Microscale laser shock processing --- modeling, testing, and microstructure characterization, J. Manufacturing Processes 3(2), 128-143.

[9] Assay, James R. and Shahipoor, M. (1992) High-pressure Shock Compression of Solids, New York, Springer-Verlag, 8-12.

[10] Johnson, G. R., Hoegfeldt, J. M., Lindholm, U. S. and Nagy, A. (1983)Response of Various Metals to Large Torsional Strain Over a Large Range of Strain Rates, J. Eng. Mat. Techn. 105, pp. 42-53.

[11] Steinberg, D. J., Cochran, S. G., and Guinan, M. W. (1980) A constitutive model for metals applicable at high strain rate, J. Appl. Phys.51(3), 1498-1504.

[12] Ungar, T., *et al.* (1984) X-ray line-broadening study of the dislocation cell structure in deformed [001]-orientated copper single crystals, Acta Metall. 32(3), 332-342.

[13] Lipkin, J. and Asay, J. R. (1977) Reshock and release of shock-compressed 6061-T6 aluminum, J. App. Phys. 48, 182-189.

Meet the Authors

Yajun Fan is a Ph.D candidate in the department of Mechanical Engineering at Columbia University. He received a MS in Materials Science from Pennsylvania State University in 2003.
Youneng Wang is a Ph.D candidate in the department of Mechanical Engineering at Columbia University.
Sinisa Vukelic is a PhD student in the department of Mechanical Engineering at Columbia University.
Y. Lawrence Yao is a Professor in the Department of Mechanical Engineering at Columbia University. He received his Ph.D. from the University of Wisconsin-Madison in 1988. He is interested in multidisciplinary research in manufacturing and design, nontraditional manufacturing processes and laser materials processing. He serves on the Board of Directors of LIA.